Experimental Study of Gust Effects on Micro Air Vehicles

Sam Zarovy[1] and Mark Costello[2]
Georgia Institute of Technology, Atlanta, GA, 30332, USA

Ankur Mehta[3] and Anita Flynn[4]
University of California, Berkeley, Berkeley, CA, 94720, USA

Greg Gremillion[5], Derek Miller[6], Badri Ranganathan[7], and J. Sean Humbert[8]
University of Maryland, College Park, MD, 20742, USA

and

Paul Samuel[9]
Daedalus Flight Systems, LLC, Rockville, MD, 20850, USA

Micro air vehicles have great potential for both civilian and military applications, but for successful deployment they must operate robustly in real world environments including flight in winds. An experimental study was performed to quantify the performance of a micro coaxial helicopter in realistic wind conditions. The experimental study evaluated different representative scenarios including: hover, forward flight, and landing on the edge of a rooftop. Each scenario was flight tested in nominal no wind cases and different wind levels. A synthetic wind generation system was used to create wind disturbances, and digital anemometers were used to measure wind magnitude and velocity at discrete spatial points. A motion capture system was used to measure vehicle position and attitude during flight tests as well as provide feedback for a conventional autopilot. Results show dramatic performance degradation in all wind environments. Flight observations reveal the micro coaxial helicopter could successfully operate in light winds with magnitudes of less than 2 m/s.

I. Introduction

With the increasing availability and functionality of small electronics today, more efforts are being focused on the design, fabrication, and operation of micro air vehicles (MAVs)—platforms on the scale of hundreds of grams and less. It is envisioned that these vehicles will operate indoors in relatively small complex spaces and outside near the ground among buildings and other structures. Within these environments a plethora of applications have been envisioned for MAVs in both civilian and military sectors[1]. The small size and relative covertness of MAVs make them ideal for reconnaissance, targeting, tagging and tracking, and internal space mapping in high risk areas that may be dangerous to humans. Moreover their high maneuverability can be employed to explore small complex spaces such as inside damaged buildings[2].

[1] Graduate Research Assistant, School of Aerospace Engineering, Student Member AIAA.
[2] Sikorsky Associate Professor, School of Aerospace Engineering, Associate Fellow AIAA.
[3] Graduate Researcher, Department of Electrical Engineering and Computer Science.
[4] Research Engineer, Department of Electrical Engineering and Computer Science.
[5] Graduate Research Assistant, Department of Aerospace Engineering.
[6] Graduate Research Assistant, Department of Aerospace Engineering.
[7] Graduate Research Assistant, Department of Aerospace Engineering.
[8] Assistant Professor, Department of Aerospace Engineering, Senior Member AIAA.
[9] President and Senior Engineer, Professional Member AIAA.

The aerodynamic velocity field near the ground, around buildings and trees, and even inside buildings is notoriously complex with the mean wind varying spatially and temporally. These flow fields consist of many features including velocity shears, vortices, separated flow, and recirculating eddies which create sharp changes in mean wind magnitude and direction over small distances[3]. Seemingly benign indoor environments can also appear gusty to a small hovering MAV due to temperature differences, openings such as windows and doors, and mechanical sources such as fans and ventilation systems[4]. These sources create significant air flows with velocities as high as 5 m/s[5,6] and spatial velocity perturbations can be on the same order of magnitude as the maximum flight speed of the vehicle leading to stall, large roll/pitch/yaw angle perturbations, and even loss of control.

While MAV gust response is a relatively new area of research, manned aircraft have been employing gust alleviation techniques since the first flights. Fixed wing aircraft have been using methods such as special direct lift control surfaces and autonomous control systems for both active and passive gust rejection for many years[7-9]. However, traditional fixed wing aircraft atmospheric disturbance modeling such as the von Karman and Dryden models usually assume a time independent or spatially frozen disturbance pattern[10] which is inadequate to represent the complex aerodynamic velocity fields MAVs expect to encounter. Active digital control technologies and structured software design have been employed to tailor control laws of rotorcraft operating near and on the decks of NAVY LHA-class ships in the presence of unsteady time varying air wakes[11]. These control strategies improve vehicle operational effectiveness in a complex environment and have the potential to be applied to MAVs.

Even with a substantial literature base on gust alleviation of manned aircraft and the velocity fields inside and outside buildings, there is little quantitative information reported on the response of MAVs operating in wind environments. The work reported here seeks to begin to fill this void by considering the response of an autonomous micro coaxial helicopter performing several prototype maneuvers in a gusty environment. A set of experiments was performed inside a motion capture facility with gust generation capability. These experiments include autonomous hover, forward flight, and landing on a roof top. Each prototype maneuver was repeated a sufficient number of times so that statistics could be generated. A set of metrics is proposed for each prototype maneuver that adequately captures vehicle performance. The paper begins with a description of the experimental apparatus followed by a description of each prototype maneuver. This is followed by a description of experimental findings and overall conclusions from the study

II. Experimental Set-up

The following subsections provide information on the major equipment used to perform the experimental study. This includes a MAV test platform, an electronics package for wireless communication, a gust generation system, and the Indoor Flight Facility— a motion capture facility where all experiments were performed.

A. Micro Coaxial Helicopter

A commercial off-the-shelf remote controlled Walkera© micro coaxial helicopter (Fig. 1) was used for all experiments. This vehicle possesses inherent stability and simplicity, weighs 55 grams, has a main rotor diameter of 175 mm with two blades per rotor, a stabilizer bar above the rotor blades, and four control inputs: throttle, pitch, roll, and yaw. As seen in Fig. 1, the helicopter has been outfitted with spherical retro-reflective markers for use in the motion capture system and also has a tail rotor which is not controllable.

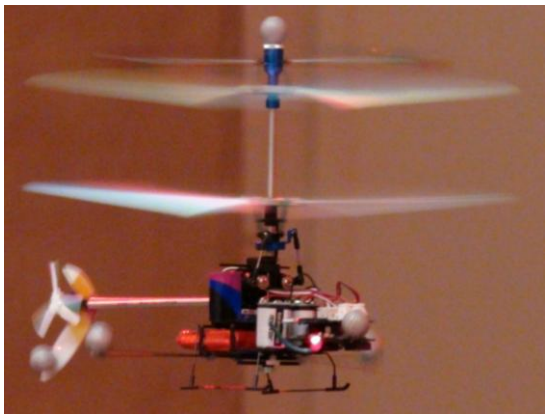

Figure 1. Walkera © micro coaxial helicopter hovering in the Indoor Flight Facility.

B. Electronics Communication Unit

The micro coaxial helicopter has been integrated with a wireless IMU circuit card called the "GINA Mote" developed by the University of California, Berkeley[12] (Fig. 2a). This mote provides wireless communication as well as control of servos and motors. Information is transmitted to and from the vehicle without recourse to tethers using a USB base station (Fig. 2b). The GINA mote also has the capability to data-log inertial information and power consumed by the vehicle.

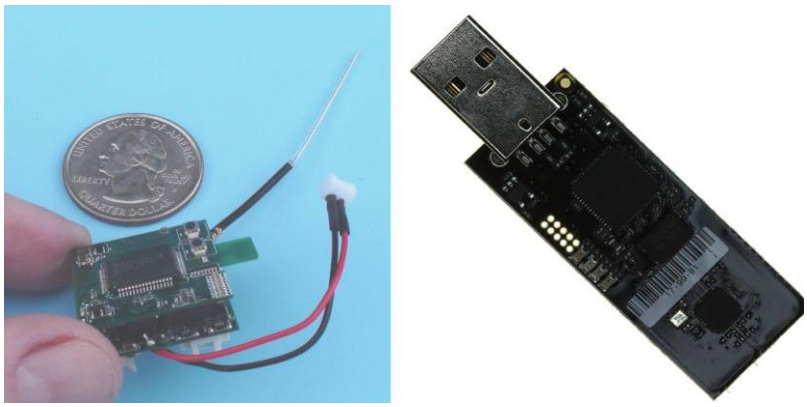

(a) (b)

Figure 2. GINA 2.0 Mote and base station. *(a) Wireless IMU GINA 2.0 Motes (b) USB wireless base station dongle.*

C. Motion Capture System

The Indoor Flight Facility (IFF) at Georgia Tech consists of a twelve camera VICON motion capture system, see Fig. 3. The infrared cameras use 3D optical position analysis to calculate the position of spherical retro-reflective markers to within 1 mm accuracy. In real time the marker positions are used to calculate position and attitude of vehicle. Using filters, state derivatives can be calculated thus allowing full state feedback of the vehicle to be recorded. Motion capture systems have been established as valuable tools in the testing of real time autonomous vehicles, control algorithm development, system identification, and testing new sensor suites[13]. This system allows the flexibility and space to construct realistic mission environments and study MAV performance in such conditions.

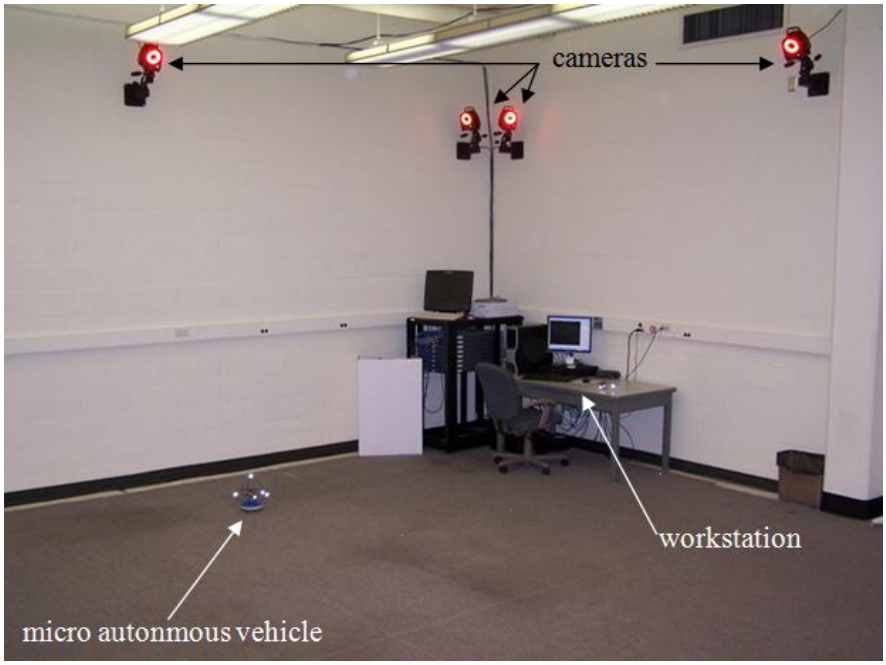

Figure 3. Indoor Flight Facility with VICON motion capture system.

D. Synthetic Gust Generation

A synthetic gust generator has been constructed (Fig. 4a) to generate accurate and repeatable conditions MAVs are likely to encounter. It is composed of a bank of eight COTS floor fans connected to a single variable transformer which enables the speed of all eight fans to be controlled simultaneously. Kestrel © Pocket Wind Meters (Fig. 4b) were used to measure wind speed and direction. These sensors use a digital anemometer to measure wind speed and a weather vane combined with a magnetometer to measure wind direction. The wind field was sampled at two second intervals and the data is logged internally. In order to characterize the wind field, measurements of wind velocity were taken at a set of discrete points in space using the motion capture system to measure sensor location. Using the data collected a statistical model of the velocity field was generated by calculating the mean and variance of wind speed and direction at each spatial point.

(a) (b)

Figure 4. Synthetic gust generation equipment. *(a) COTS fans bank (b) Kestrel © Pocket Wind Meter.*

III. Experimental Description

The set of experiments was designed to quantitatively characterize MAV platform responses to a variety of basic wind environments, with the aim to perform simple yet insightful tests to gain an understanding of current MAV capability and identify gaps in platform design and control algorithm development. To this end three prototype maneuvers were flight tested: hover, forward flight, and a realistic flight maneuver—landing on a rooftop. Both hover and forward flight tests were performed in relatively smooth flow and in turbulent flow to capture differences caused by turbulence. Vehicle position and attitude were recorded from the motion capture system as were the control inputs sent to the vehicle. The control inputs were recorded as pulse-position modulation (PPM) signals which are set as values between -1 and 1 with -1 corresponding to no throttle input and 0 corresponding to neutral positions for roll, pitch and yaw inputs. This data along with some scenario specific metrics were used analyze helicopter performance in the maneuvers tested.

A. Hover

For many MAV missions the vehicle must be able to hold a level attitude and position. For hover experiments the MAV took off in little to no wind then rose into the full gust flow generated by the synthetic gust generation system, where it was commanded to hover for thirty seconds before landing (Fig. 5). A metric for hover accuracy is the spherical error probable (SEP) which is defined as the radius of a sphere that encircles 50% of the trajectory for a particular flight. The 50% SEP was calculated in post processing for each flight test. The average SEP value was calculated for all flight tests at one wind setting to compare hover performance at different wind settings.

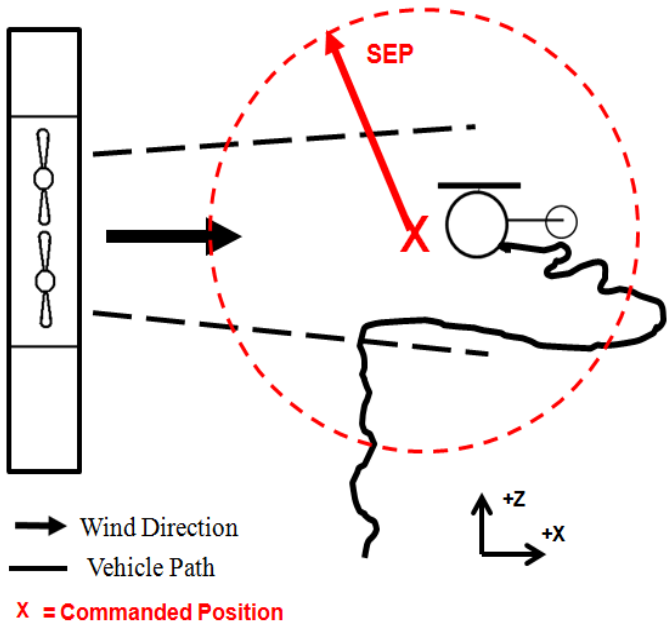

Figure 5. Illustration of MAV hover experiment.

To study the effects of turbulent flow on hover performance, an obstruction was placed in the flow (Fig. 6a) which caused distortion in the flow (Fig. 6b). The same hover flight test procedure as described above was performed at different positions in the flow with and without the obstruction in place to compare performance in smooth and turbulent flows. The four positions tested are also shown in Fig. 6b and Table 2, with position 2 being directly behind the obstruction and position 4 just above its top.

(a)

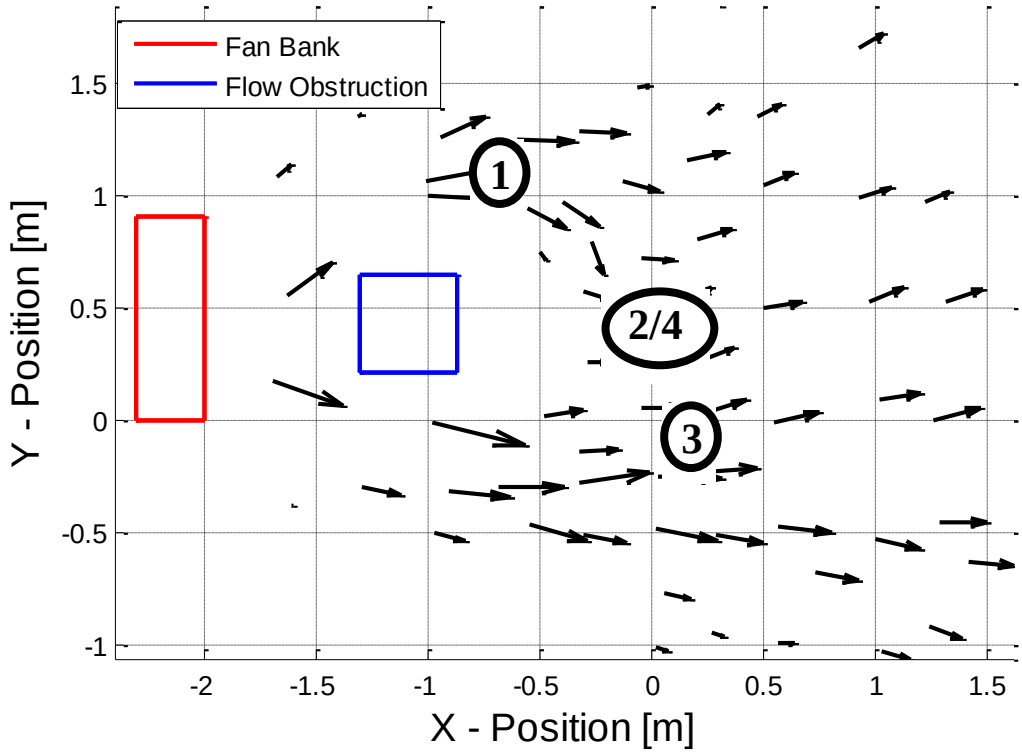

(b)

Figure 6. Hover in turbulent air. *(a) Obstruction used to create turbulent flow (b) Mean velocity field with obstruction in the flow with positions tested numbered.*

Position	X [m]	Y [m]	Z [m]
1	-0.6	1.2	1.0
2	0.0	0.45	1.0
3	0.2	-0.1	1.0
4	0.0	0.45	1.45

Table 1. Commanded positions tested for hover in turbulence experiment.

B. Forward Flight

During forward flight, gusts may cause a MAV to be blown off course. Figure 7 illustrates the forward flight experiment to quantify how a cross range gust affects the capability of the vehicle to track a commanded trajectory. A useful metric is tracking error—the shortest distance from the position of the vehicle to the desired trajectory as shown in Fig. 7. The mean maximum tracking error was recorded for all flights at a given wind speed to examine trajectory tracking performance changes with wind speed.

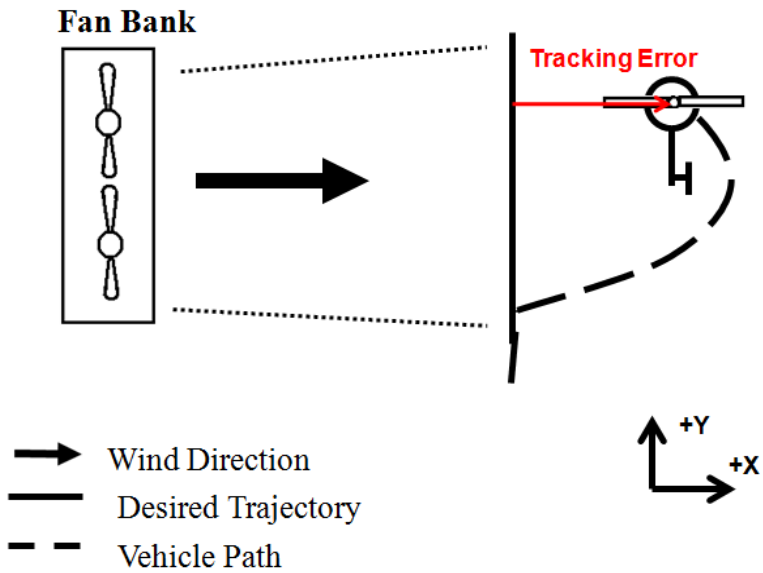

Figure 7. Illustration of MAV in forward flight.

To understand the effects of turbulence on forward flight performance the same obstruction was placed in the flow and the forward flight tests were repeated in its wake (Fig. 8). The mean maximum tracking error was again calculated at each wind level.

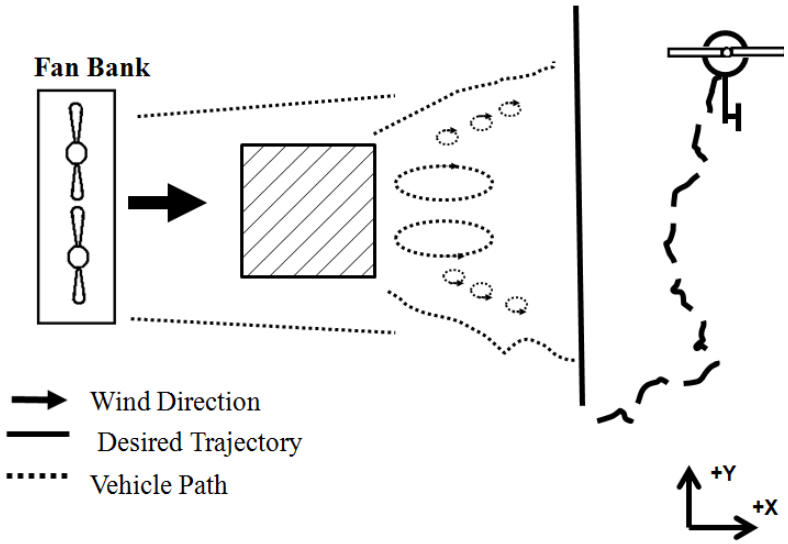

Figure 8. Illustration of MAV in forward flight in turbulent air experiment.

C. Roof Top Landing

A basic mission scenario that is often described for MAVs is landing and perching on the edge of a rooftop, which is relevant in surveillance and reconnaissance situations for military applications, or observing traffic in urban civilian applications. Figure 9a illustrates the rooftop landing experiment performed. The helicopter approached a representative rooftop platform (Fig. 9b) and landed on a target in the presence of wind.

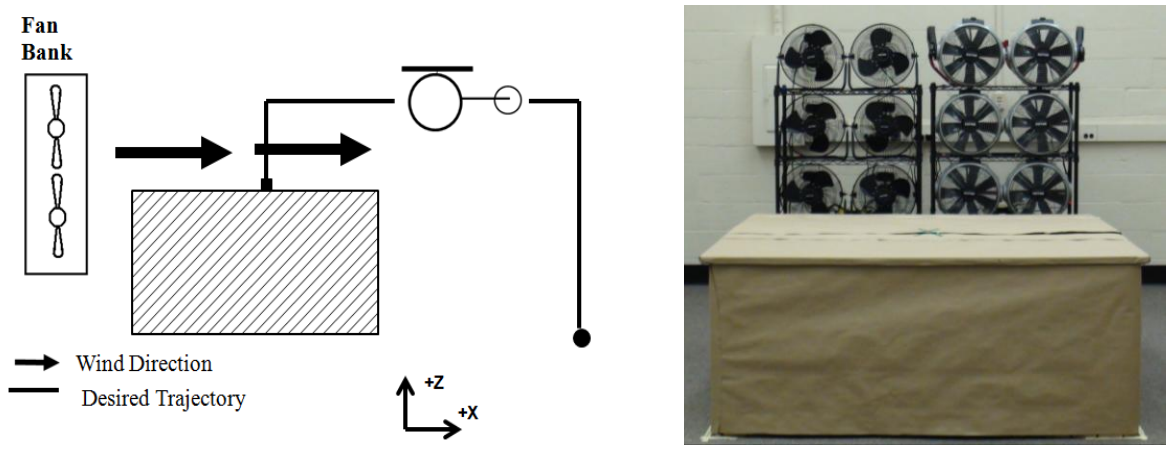

(a) (b)

Figure 9. Rooftop landing experiment. *(a) Experiment illustration (b) Constructed representative rooftop.*

To ensure the safety of the vehicle, the landing sequence was designed to occur after the helicopter had hovered over the target landing position for a set amount of time. When the helicopter was able to hover in a meter by meter square landing zone above the target for five seconds then the safe landing sequence is initiated (Fig. 10a). The landing accuracy was captured by calculating the 50% circular error probable (CEP) from the landing positions of all flight tests at a wind level. Like SEP, circular error probable is the radius of a circle that encompasses fifty percent of the test flight landing positions, see Fig. 10b.

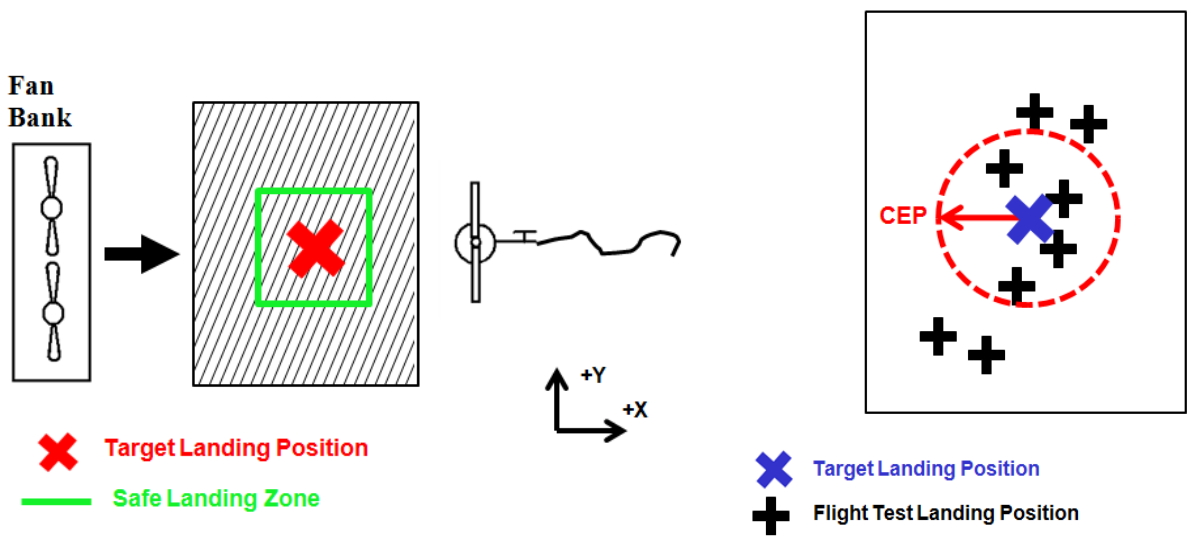

(a) (b)

Figure 10. Rooftop Experiment definitions. *(a) Safe landing zone. (b) 50% circular error probable illustration.*

IV. Autonomous Control Algorithm

Figure 11 shows a block diagram of the control algorithm used for autonomous flight during all experiments. Position and attitude measurements from the motion capture system are processed in real time. Control inputs are then calculated based on the measurements and state commands—position (x,y,z) and heading angle (ψ)—and sent to the helicopter via the USB base station dongle, Fig. 11a. The inertial position errors calculated from VICON measurements are rotated into the vehicle body frame to relate x, y, and z position errors to pitch, roll, and throttle inputs respectively. The altitude (z) and heading angle (ψ) errors feed directly into PID control gains to compute throttle and yaw inputs while the x and y body position errors are used to compute pitch (θ) and roll (ϕ) commands (Fig. 11b,c). The derivative and integral terms are calculated using second and first order discrete filters respectively and motion capture system measurements are also filtered to reduced noise. All control gains were determined experimentally and are shown in Table 2.

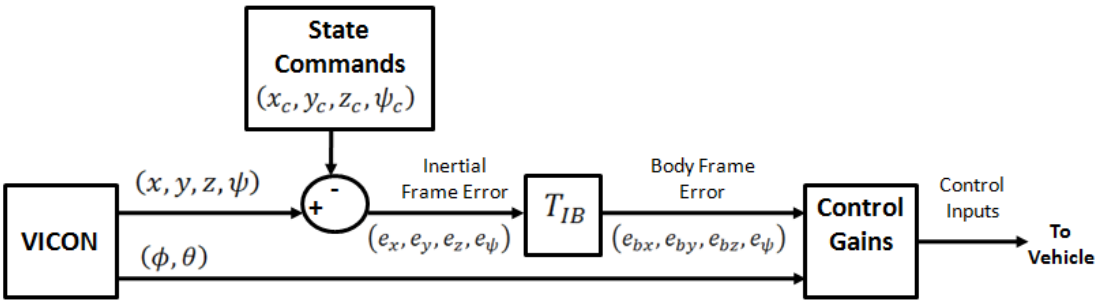

(a)

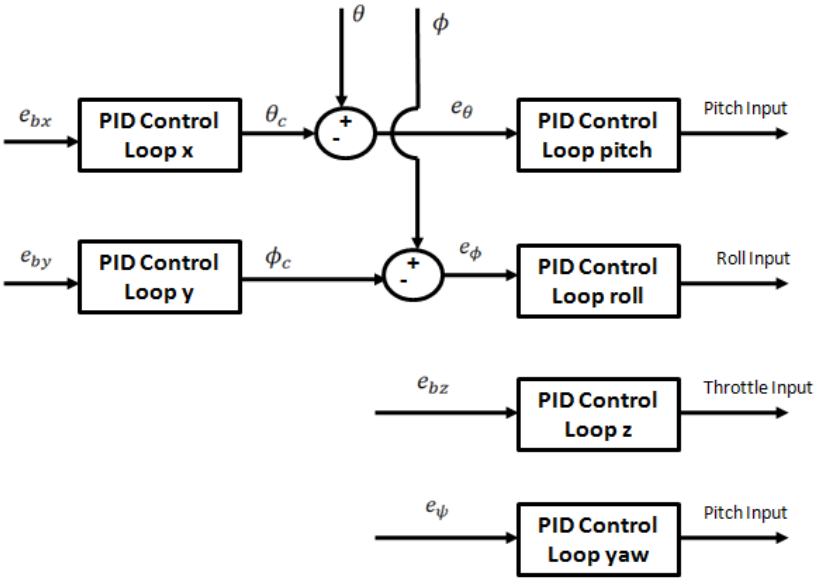

(b)

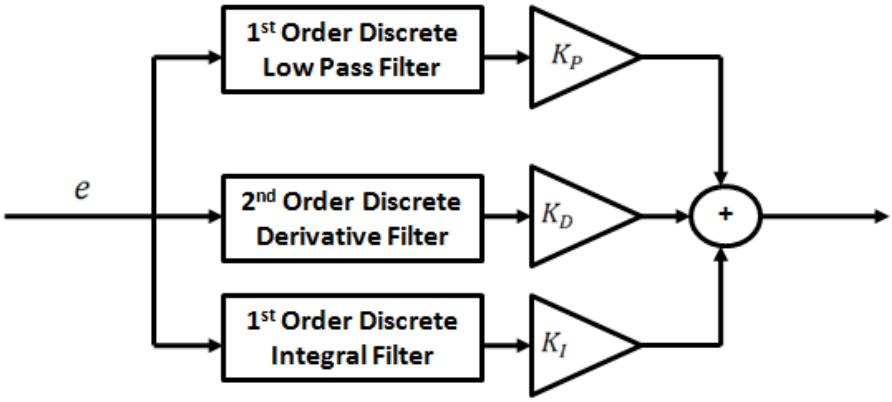

(c)

Figure 11. Autonomous control algorithm. *(a) Overview (b) Control Gains block (c) Example PID Control Loop block.*

	K_P	K_D	K_I
x	-2.00E-04	-1.00E-04	-3.00E-05
y	2.00E-04	1.00E-04	3.00E-05
z	-6.00E+04	-3.00E-04	-8.00E-05
ϕ	-0.80	0.00	0.00
θ	0.80	0.00	0.00
ψ	0.20	0.01	0.10

Table 2. Autonomous control algorithm gains.

V. Experimental Results

A. Hover

The flow field was measured at 108 spatial points for 2 minutes each and mean magnitude and direction are shown in Fig. 12a. Figure 12b shows the mean wind speed with respect to altitude at the command position which shows the increase in wind speed with starting near zero and increasing with altitude.

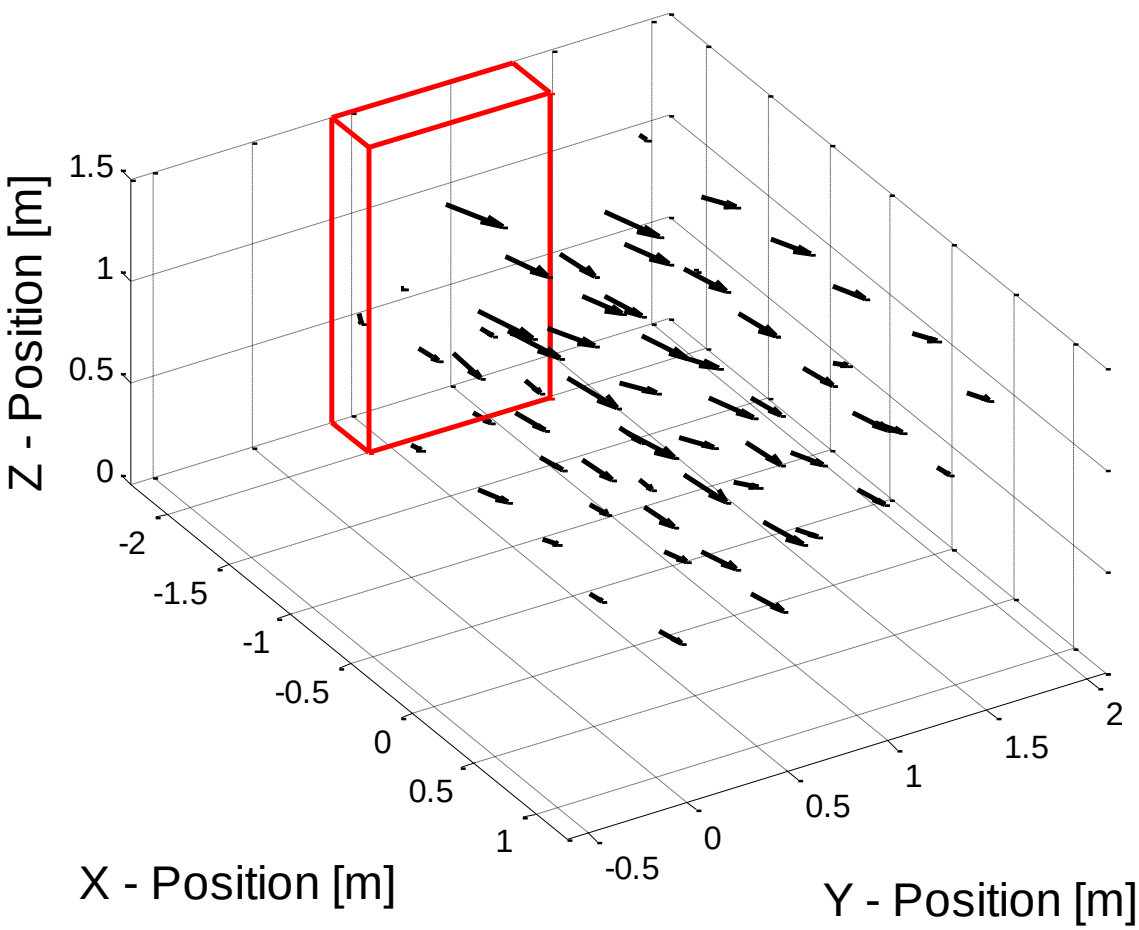

(a)

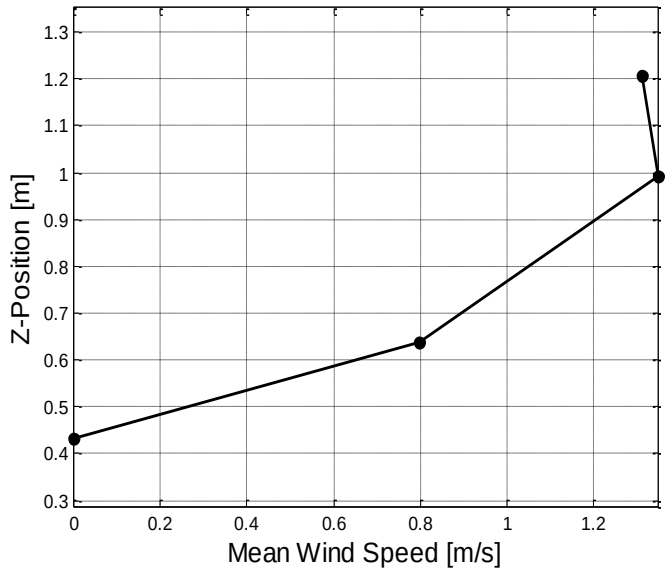

Figure 12. Flow characterization for hover experiment. (*a) Mean velocity field with the fan bank outlined in red (b) Mean wind speed with altitude at command hover position*.

Figure 13 shows example time histories of vehicle position flight trajectories for the micro coaxial helicopter in 0.0, 1.0, and 20 m/s wind which illustrate the basic behavior of the vehicle when entering a small gust. At first the helicopter was pushed downwind (positive x-direction) before the autopilot was able to compensate and return closer to the commanded hover position. Figure 14 shows an increase in vehicle vibration as wind level increases.

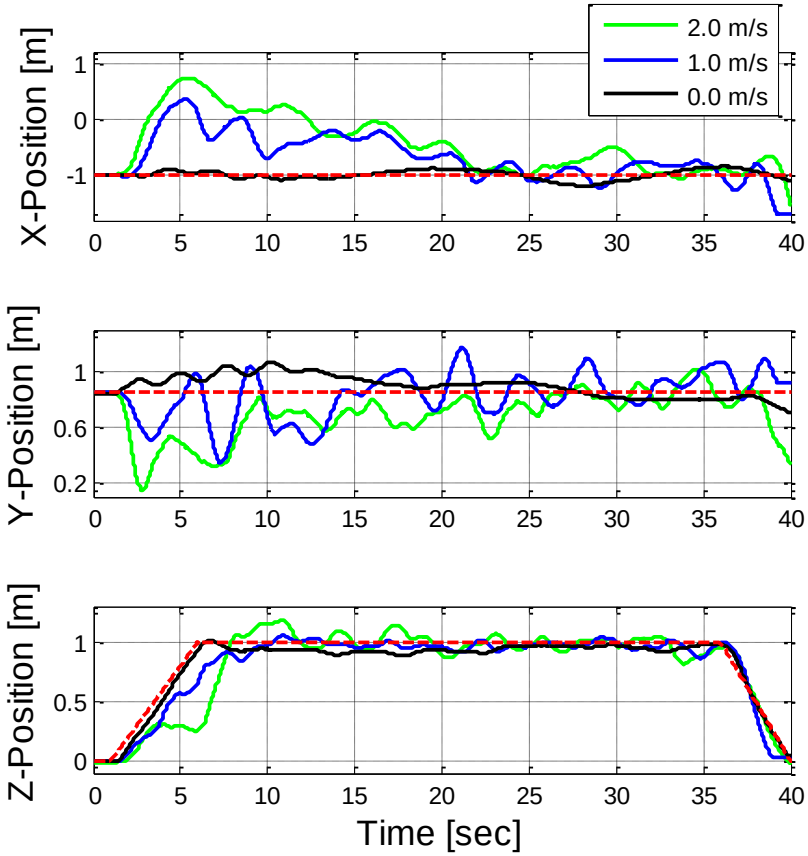

Figure 13. Example time histories of vehicle position for hover at 0.0, 1.0, and 2.0 m/s wind levels with commanded position in red.

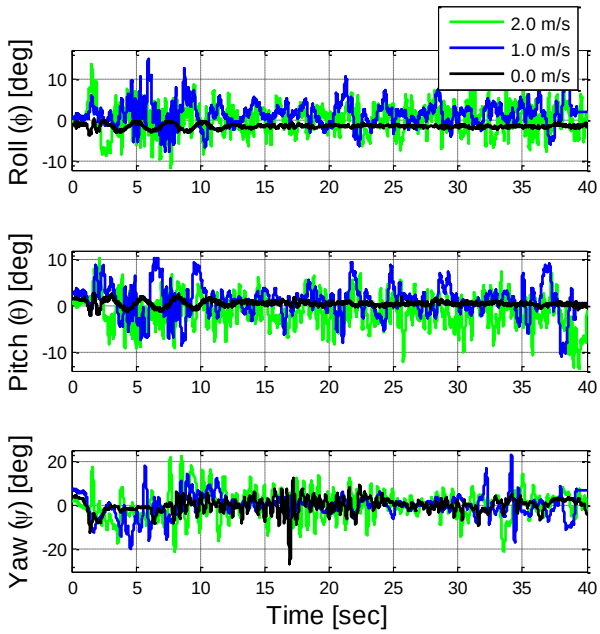

Figure 14. Example time histories of vehicle attitude in hover for 0.0, 1.0, and 2.0 m/s wind levels.

From Fig. 15 it can be seen that the control input required to maintain commanded hover position increases drastically in magnitude and frequency for increasing wind levels. This significant change in control input suggests an increase in power consumption in windy conditions which would reduce endurance of the vehicle. Also it should be noted that for one and two m/s wind levels the throttle input saturates at the upper limit of one PPM, which is shown in more detail in Fig. 16, where the actual saturated control is compared to the desired control computed by the autopilot. Figure 16 shows that for a 2 m/s wind level the throttle input calculated by the autopilot was almost twice the limit.

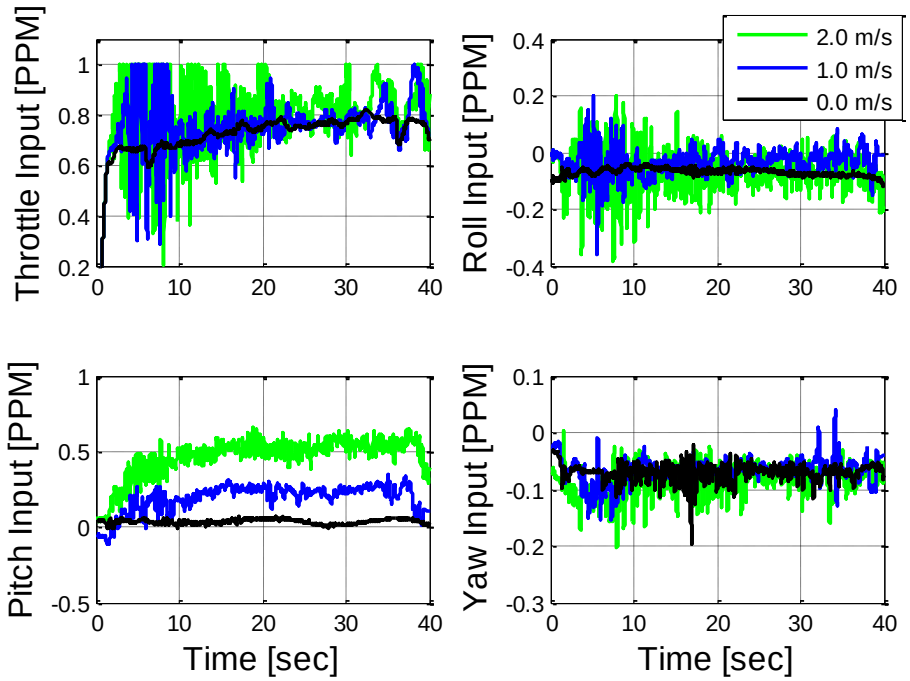

Figure 15. Example time histories of hover for vehicle control inputs in 0.0, 1.0, and 2.0 m/s wind levels.

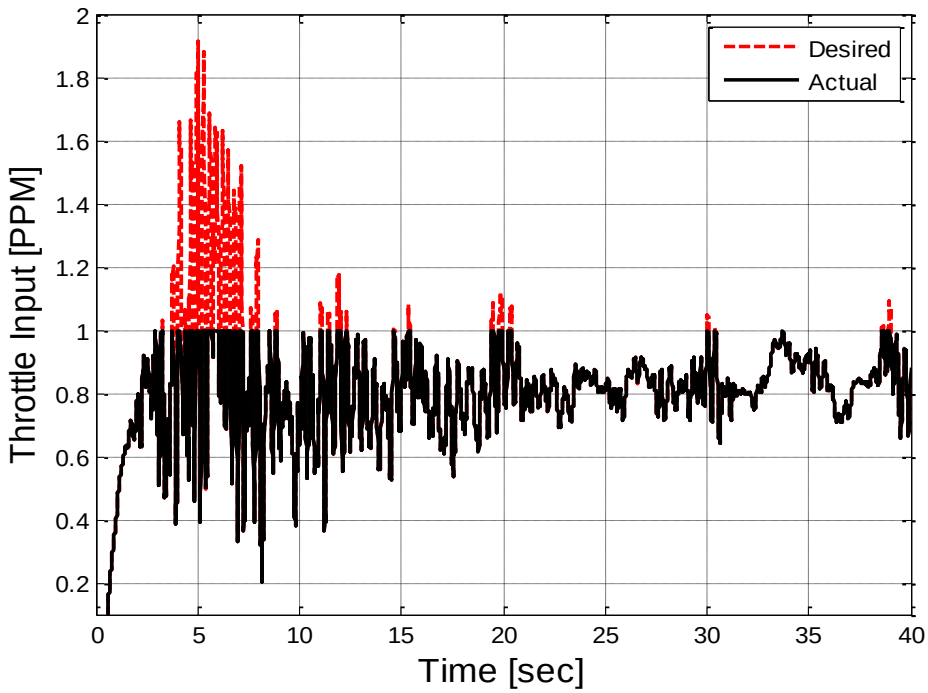

Figure 16. Example time history of desired and saturated throttle input in 2.0 m/s wind.

Figure 17 shows the average SEP values at each wind level test with 95% confidence error bars, and as expected the ability of the vehicle to maintain hover at a commanded position decreases as the wind level increases with the SEP at 2 m/s at least 3 times larger than the SEP in no wind.

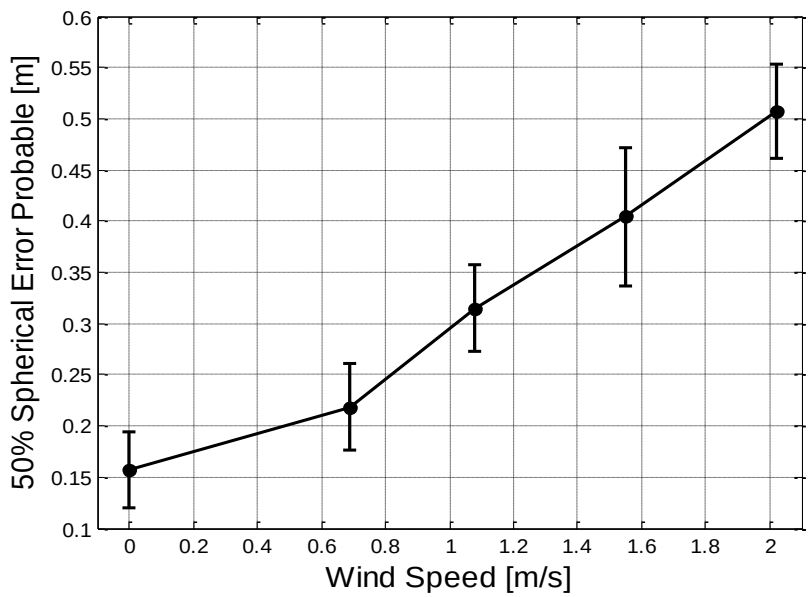

Figure 17. Average 50% spherical error probable (SEP) for each wind level tested with error bars for 95% confidence.

Quantitatively capturing the hover performance of the helicopter in turbulent flows generated by placing an obstruction in the flow proved difficult. Safety precautions such as ensuring the vehicle would not strike the box or be blocked from view of the VICON cameras limited how close the helicopter was allowed to fly to the obstruction and the number of test flights performed. Table 3 shows the average SEP values in both smooth and turbulent flows at positions 1, 3, and 4.

	50% SEP [m]	
Position	Smooth	Turbulent Air
1	0.372 ± 0.083	0.475 ± 0.096
3	1.306 ± 0.098	1.373 ± 0.141
4	0.841 ± 0.168	0.677 ± 0.067

Table 3. Average 50% spherical error probable at position tested in smooth air (no obstruction) and turbulent air (obstruction in place) with 95% confidence.

At position 2—directly behind the box—not enough successful flight tests could be completed to form statistics. As seen in Fig. 6 the magnitude of the wind is small directly behind the obstruction, thus when the helicopter was blown downwind in the x-direction and slowly returned to position 2 the wind field changed rapidly causing the vehicle to crash into the obstruction. Of the ten test flights performed at position 2 the vehicle crashed in eight due to overcompensation of the wind. Figure 18 shows an example time history of the x-position of the vehicle during a flight test at position 2 with the blue arrow indicating the area of rapid wind change and the red arrow indicating the crash with the obstruction.

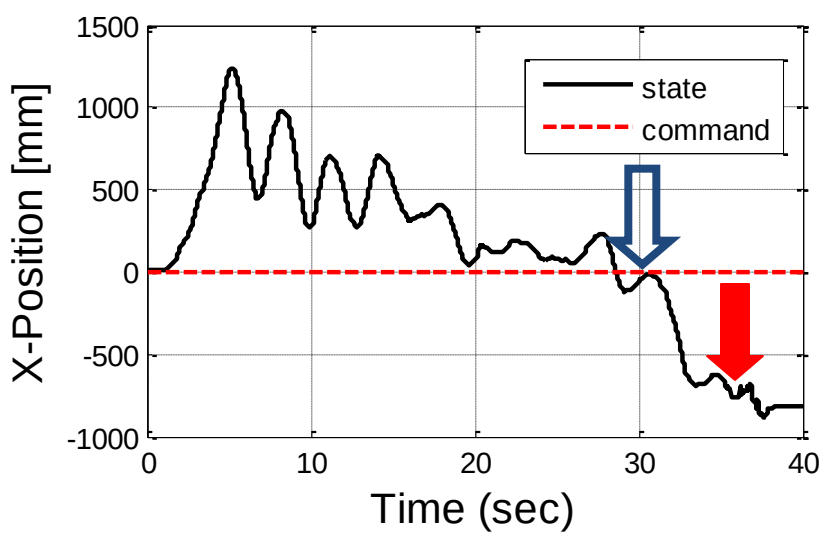

Figure 18. Example time history of vehicle x-position at position 2. *The blue arrow indicates the region of rapid wind velocity change and the red arrow indicates the vehicle contacting the obstruction.*

As shown in Table 3, at positions 1 and 3 (near the corners of the obstruction) the ability of the helicopter to hold a commanded hover position decreased in turbulent flow. It was observed that during flight tests in turbulent flow the vehicle vibrated at a much high frequency which can be seen for position 1 in Fig. 19. Figure 20 shows a partial time history of vehicle roll angle which shows a closer view of the high frequency response of the helicopter in turbulent flow. Time histories at position 3 show similar characteristics but much lower in magnitude (Fig. 21). It is clear at positions 1 and 3 the vehicle experiences turbulence created by the obstruction, but since position 3 is farther away from the obstruction the turbulence is smaller in magnitude. In both positions turbulent flow is shown to degrade the ability of the vehicle to maintain hover.

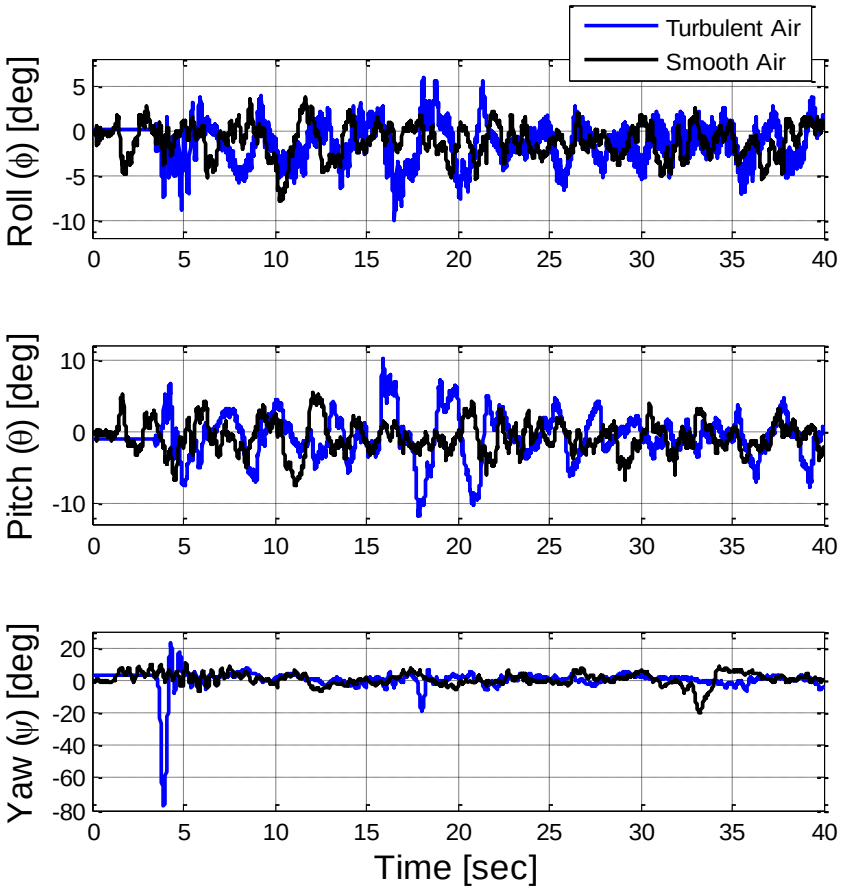

Figure 19. Example time histories of vehicle attitude for turbulent and smooth air at position one.

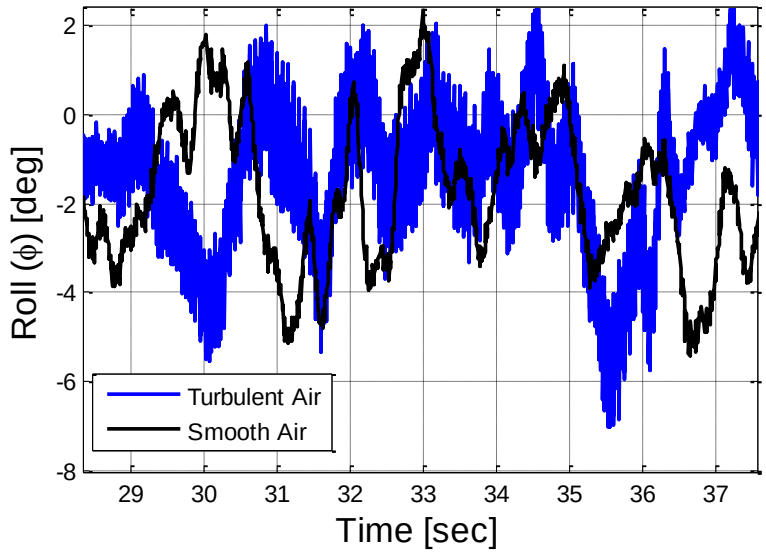

Figure 20. Example partial time histories of vehicle roll attitude for turbulent and smooth air at position one.

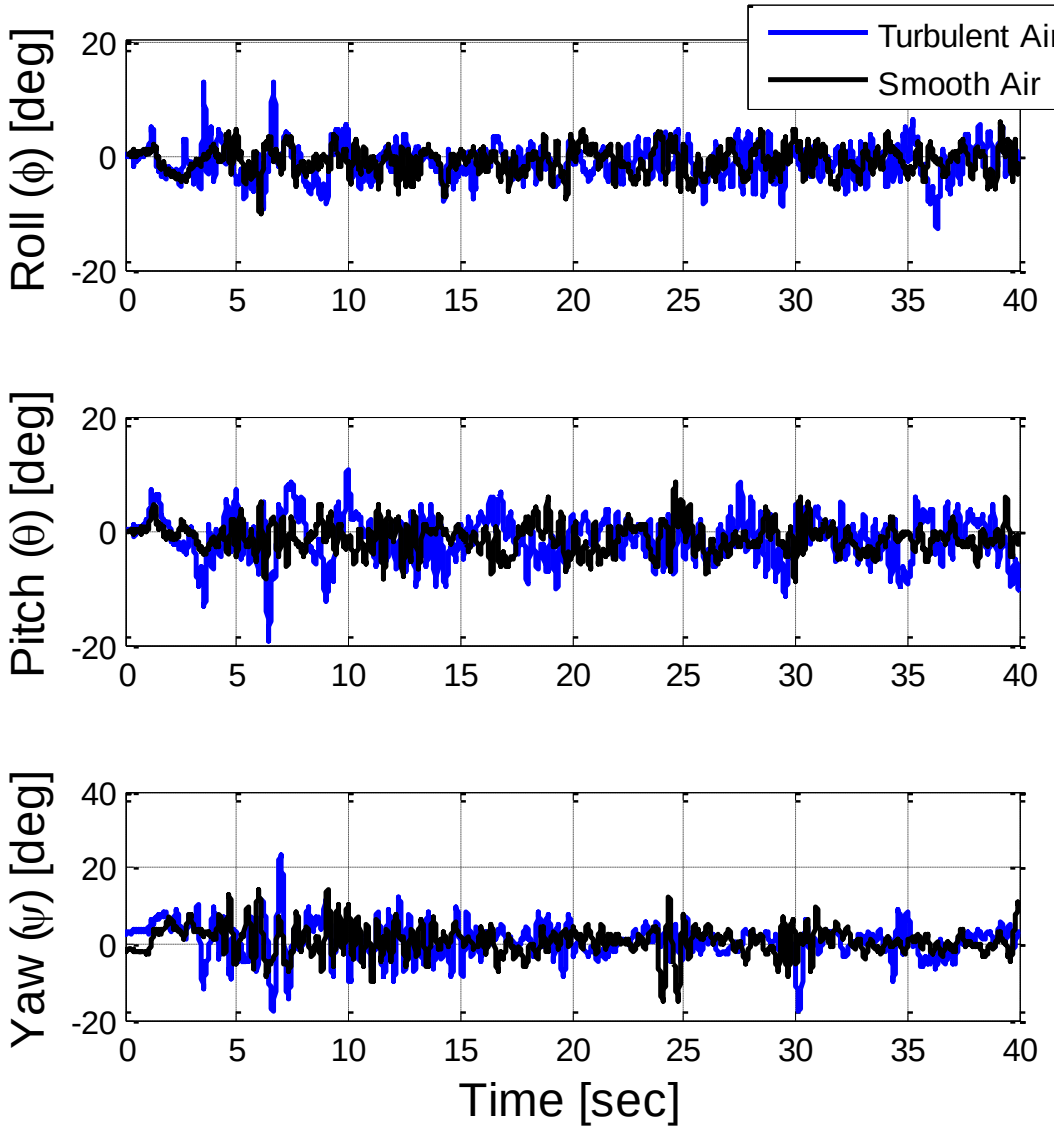

Figure 21. Example time histories of vehicle attitude for turbulent and smooth air at position three.

Flight tests showed hover performance of the vehicle at position 4 was improved when the obstruction was placed in the flow. Behind and slightly above the obstruction, position 4 saw a reduction in the wind magnitude much like position 2. The flow at position 4 may have not been as turbulent as at positions 1 and 3 and this combined with a reduced wind field could have made flow around position 4 calmer than without the obstruction in place. Figure 22 plots an example time history of the vehicle attitude at position 4 which shows the response to smooth and turbulent air to be very similar unlike the other positions tested.

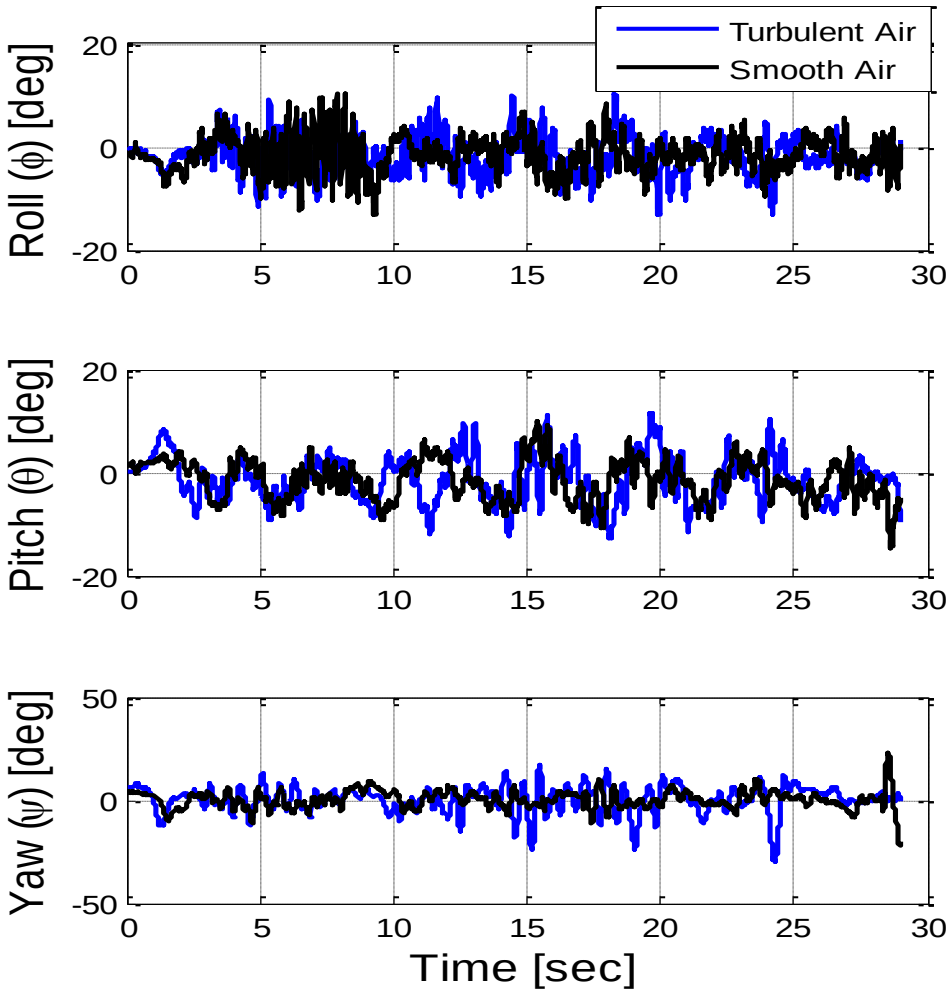

Figure 22. Example time histories of vehicle attitude for turbulent and smooth air at position four.

B. Forward Flight

The mean velocity field is shown in Fig. 23a. The synthetic gust generation system creates a large magnitude gust where the fan bank was positioned—at y-position 0 m—while the air velocity at the test starting position—at y position -1.0 m—is almost zero, as seen in Fig. 23b. Flight tests were performed at wind levels of 0.0, 0.6, 0.83, 0.91, 1.2, and 1.54 m/s.

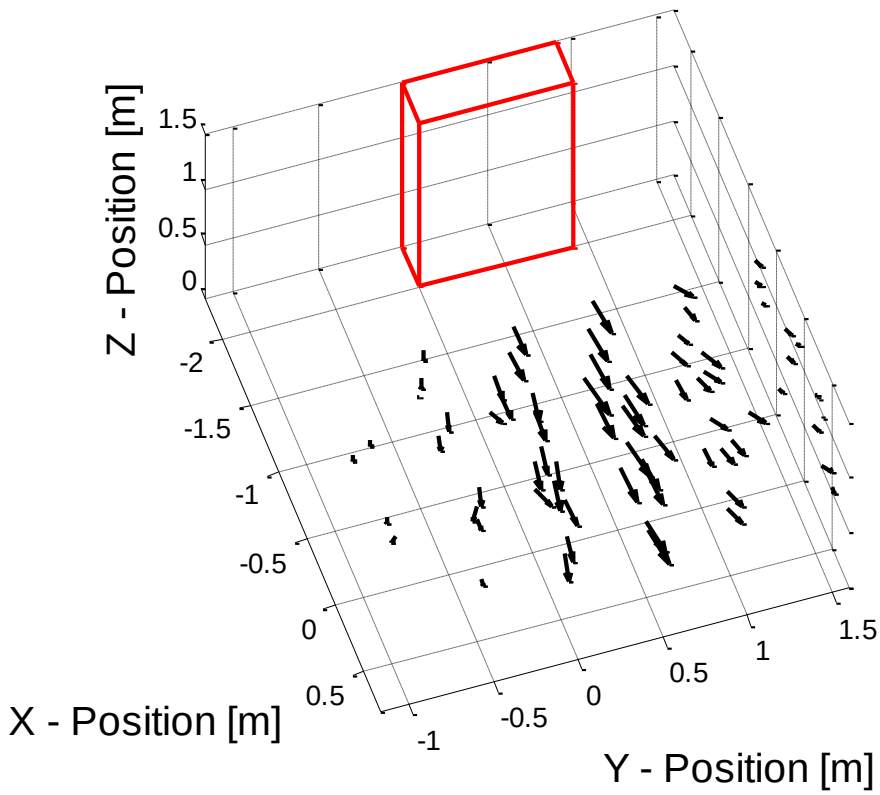

(a)

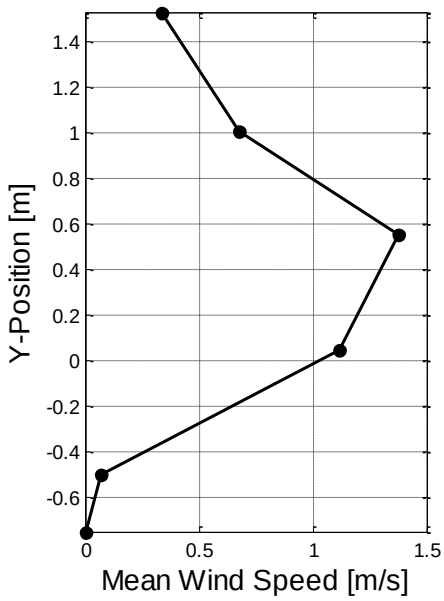

(b)

Figure 23. Flow characterization for forward flight. *(a) Mean velocity field with the fan bank outlined in red (b) Mean wind speed with y-position along the commanded trajectory.*

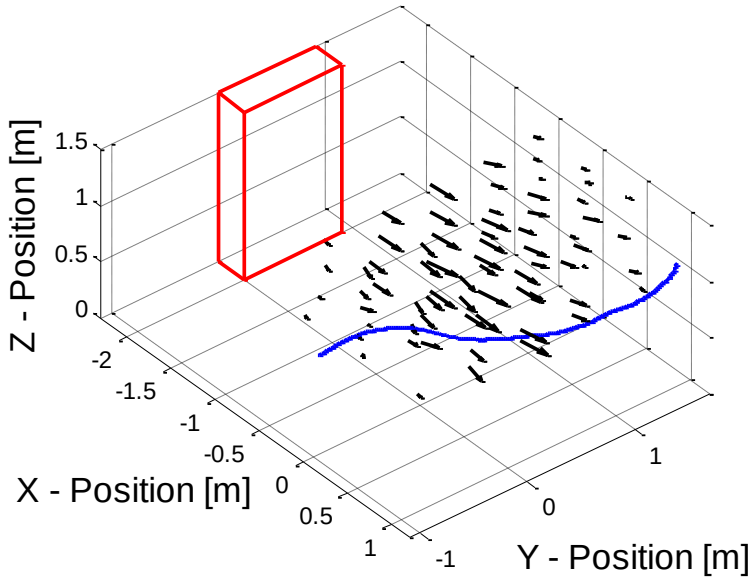

Figure 24. Example flight trajectory (blue) overlaid with measured flow field at 1 m/s wind (black arrows) generated from gust generation system (red outline).

Figure 24 shows an example flight trajectory at one m/s wind overlaid with the corresponding measured flow field. As expect when the vehicle encounters the cross wind gust it is blown perpendicular to the commanded course. The synthetic gust generation system was centered at y-position of 0.4 m, and as can be seen in Fig. 23b the wind magnitude is relatively low between -1 and -0.5 m in the y-position. Then the wind velocity increases to almost full speed between 0 and 0.8 m before decreasing again. Thus as Fig. 25 shows, the tracking error starts to increase noticeably as the vehicle approaches a y-position of 0 m and the maximum tracking error increases with wind level. Figure 26 shows the average maximum tracking error which increased with wind level. At 1.5 m/s wind is almost eight times as large as the tracking error in no wind.

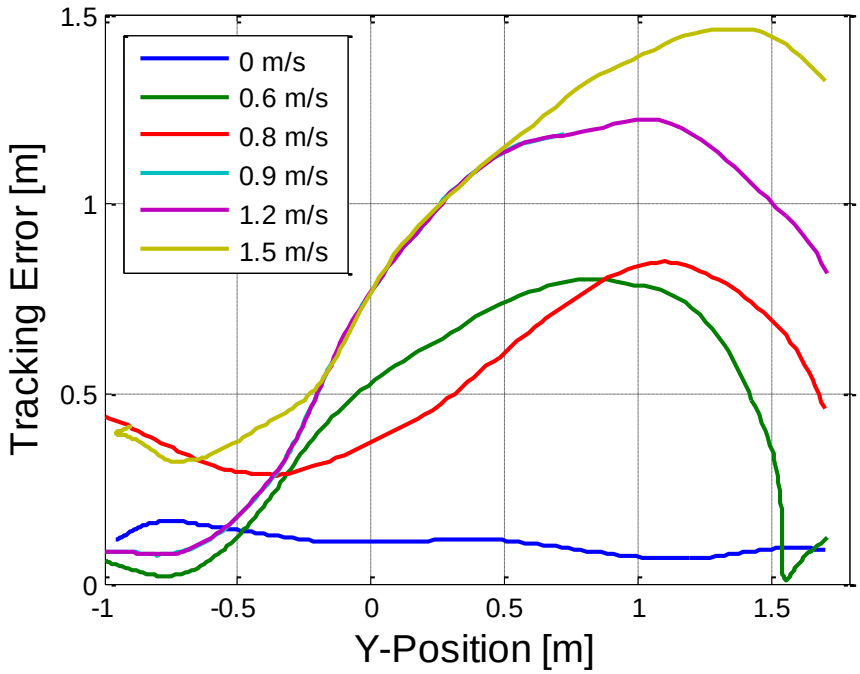

Figure 25. Tracking errors for example test flights of forward flight in smooth air.

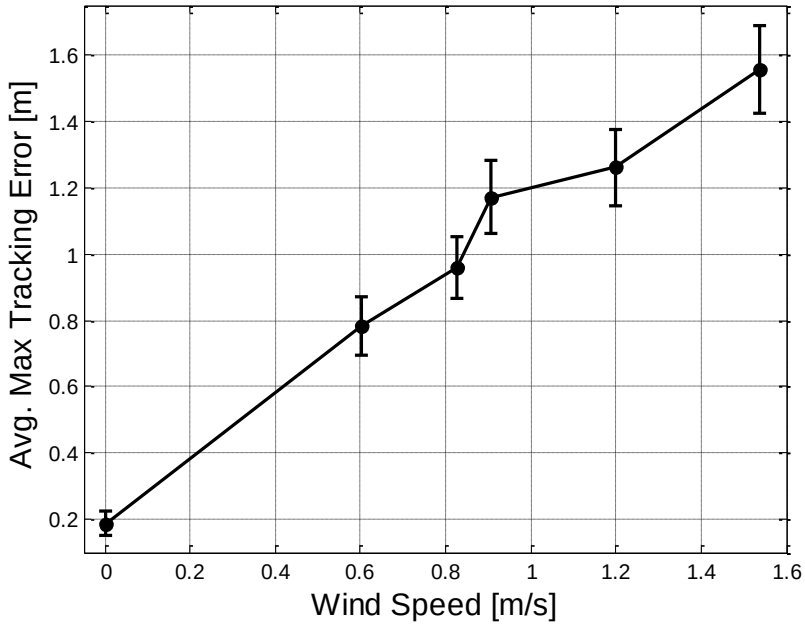

Figure 26. Average maximum tracking error of forward flight in smooth air at each wind level with 95% confidence error bars.

Control inputs again increased significantly for higher wind levels and throttle saturation occurred, see Fig. 27. This repeated saturation during forward flight compromises the gust rejection and altitude hold capabilities of the vehicle and may be one of the causes of the performance degradation.

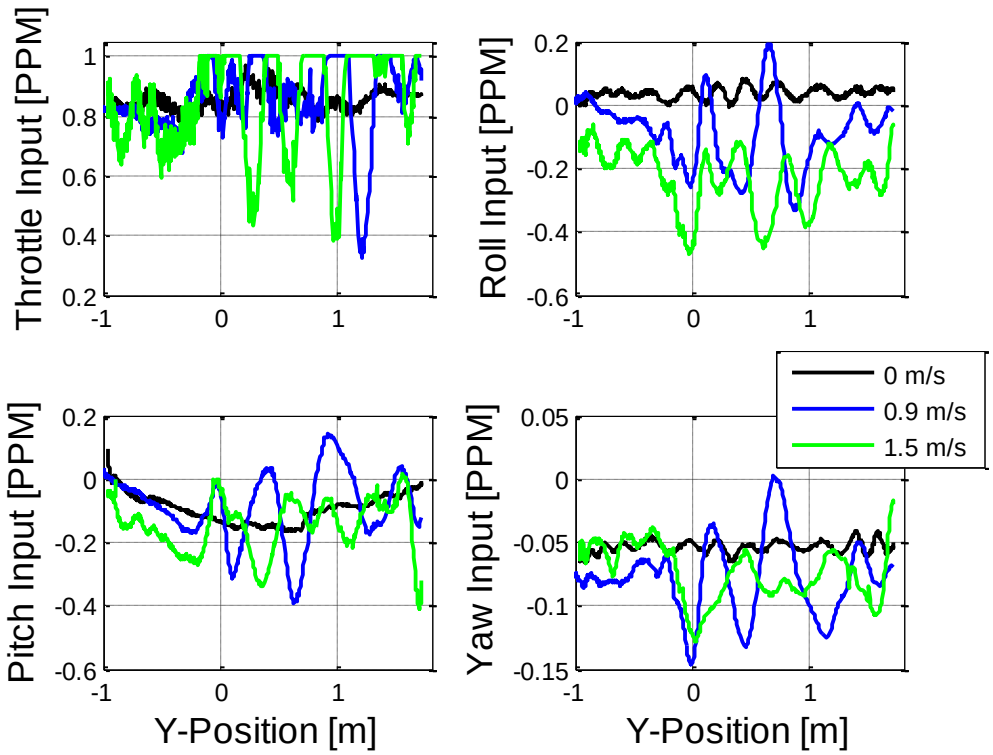

Figure 27. Example time histories of vehicle control inputs in 0.0, 0.9, and 1.5 m/s wind levels in forward flight in smooth air.

Flight tests using the obstruction to create turbulent flow showed similar gust response as in smooth air only reduced as seen by the smaller average maximum tracking error (Fig. 28) and little to no control saturation (Fig. 29). During these flight tests it was observed that as the vehicle traveled behind the obstruction it encountered a reduced wind magnitude but relatively little turbulence except at the box corners providing calmer air than the smooth air flight tests. Also the obstruction deflected air flow towards the test starting position thus increases in the flow velocities the helicopter encountered during takeoff especially during flight tests at 0.9, 1.0, and 1.2 m/s wind levels. This led to more variability in the starting forward flight positions and may account of the large error bars and similar average maximum tracking errors at those wind speeds.

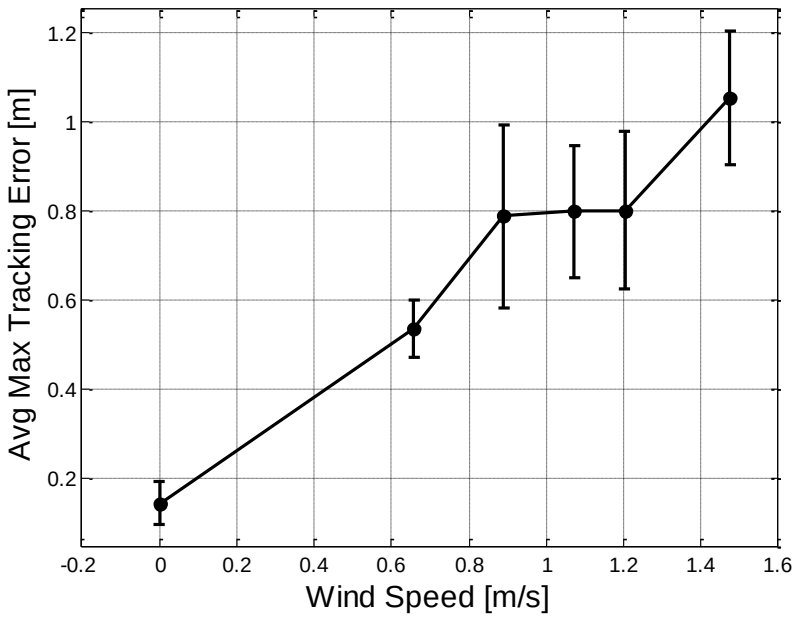

Figure 28. Average maximum tracking error of forward flight in turbulent air with 95% confidence error bars.

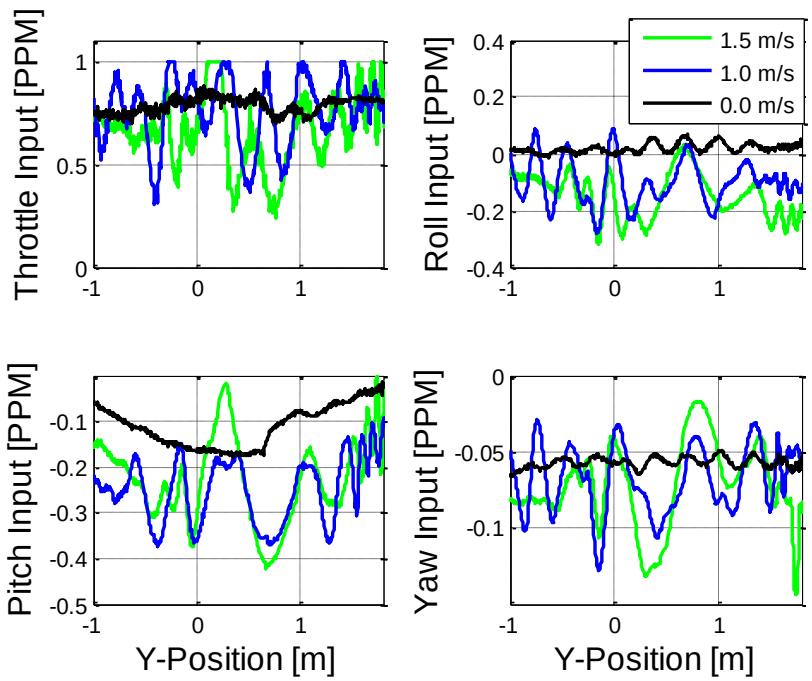

Figure 29. Example time histories of vehicle control inputs in 0.0, 0.9, and 1.5 m/s wind levels for forward flight in turbulent air.

C. Rooftop Landing

The mean spatial velocity field measured is shown in Fig. 30. It was observed that little to no wind was measured at ground level while wind speed increased with altitude.

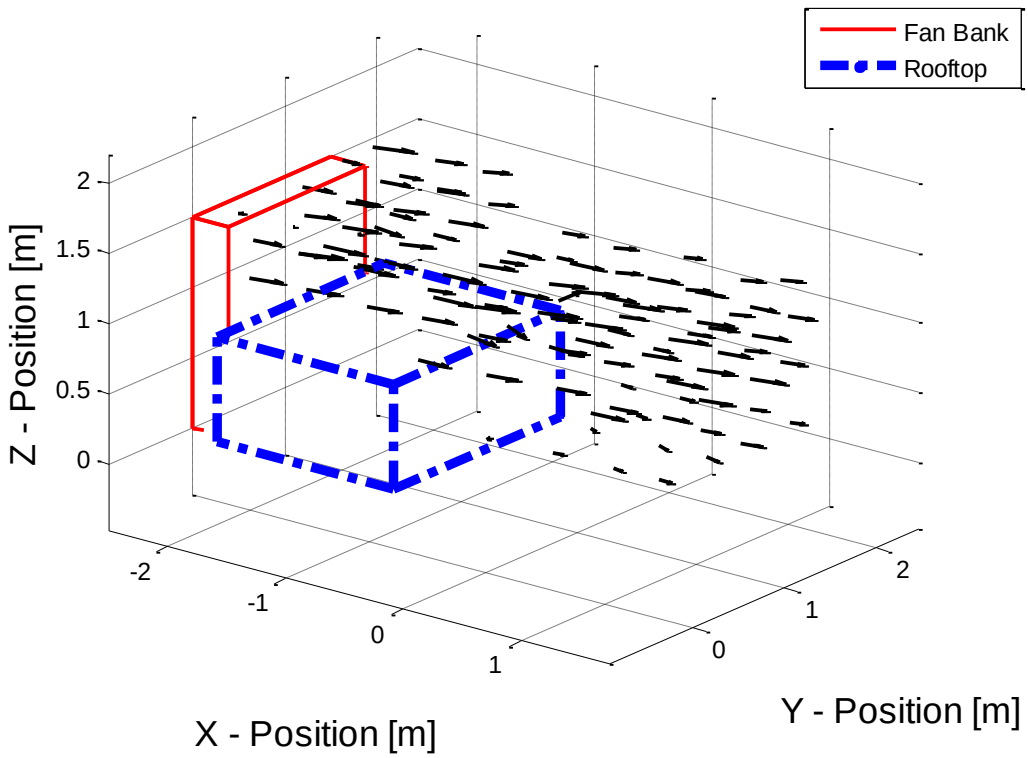

Figure 30. Flow characterization for rooftop landing. *Mean velocity field with the fan bank outlined in red and the rooftop in blue.*

Figure 31 shows example x-z state histories of test flights in 0, 0.8, and 1.2 m/s wind levels landing on the representative roof top. Results of this experiment showed very little trending in target centered average CEP values as wind levels increased, see in Fig. 32. This shows that the accuracy the vehicle to land on a target in winds is not impacted as dramatically as performance results of earlier experiments showed.

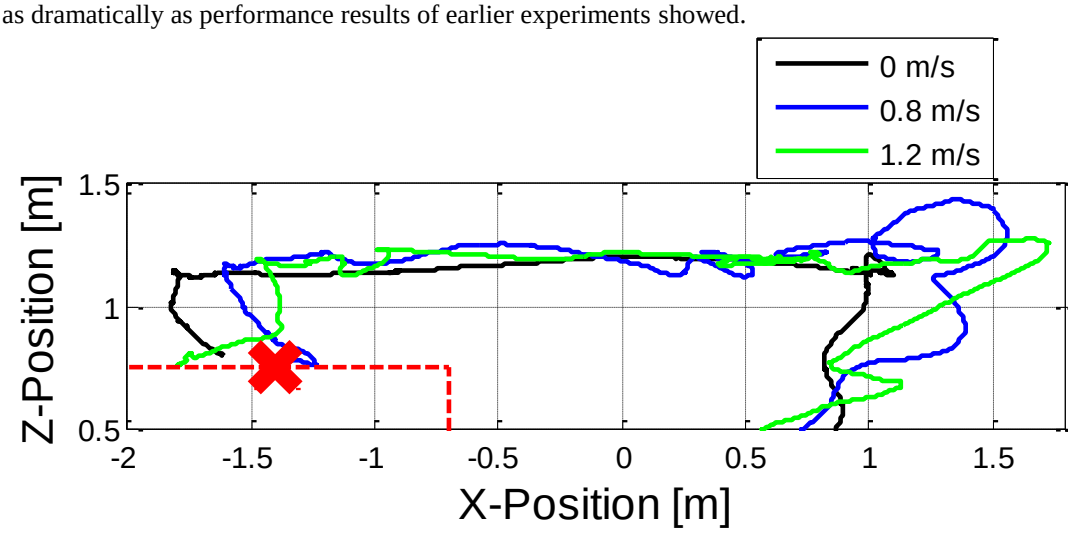

Figure 31. Example test flights of roof top landing in 0.0, 0.8, and 1.2 m/s wind levels. *The roof top is outlined as a red dotted line and target landing is shown as a red cross.*

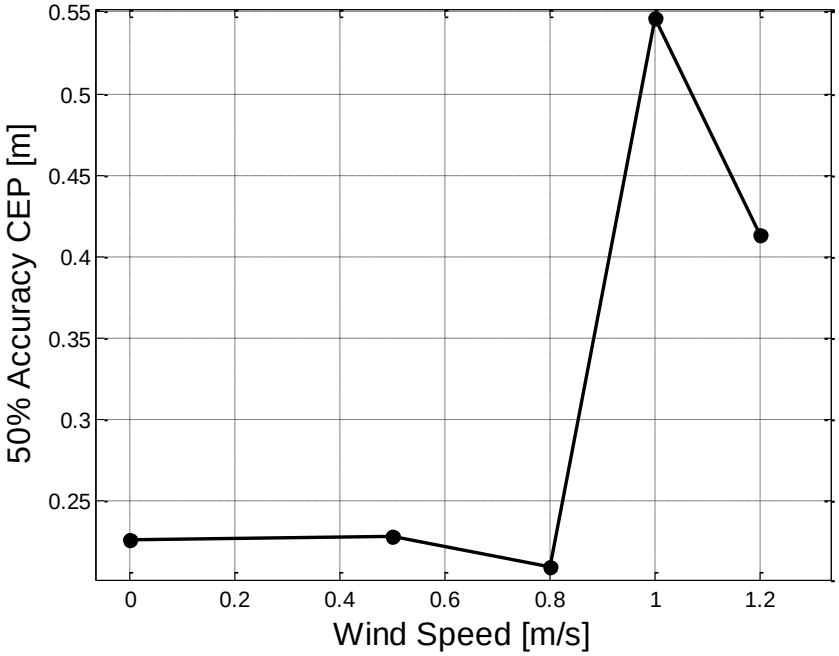

Figure 32. Accuracy 50% circular error probable of roof top landing experiment.

However further inspection of results showed that while landing accuracy may not show the expected trends in winds, the landing precision does decrease significantly in winds. Landing precision can be measured as the 50% CEP centered at the mean landing position for a given wind level. If one thinks of the landing accuracy 50% CEP is the average offset from the target, the precision CEP can be thought of was the variance, see Fig. 33. Figure 34 shows the 50% CEP for landing precision at all wind levels and as expected the ability of the helicopter to land consistently degrades as wind level increases with the CEP at 1.5 m/s wind almost five times as large as the no wind CEP. This trend reduces the ability of the helicopter to land safely in windy environments.

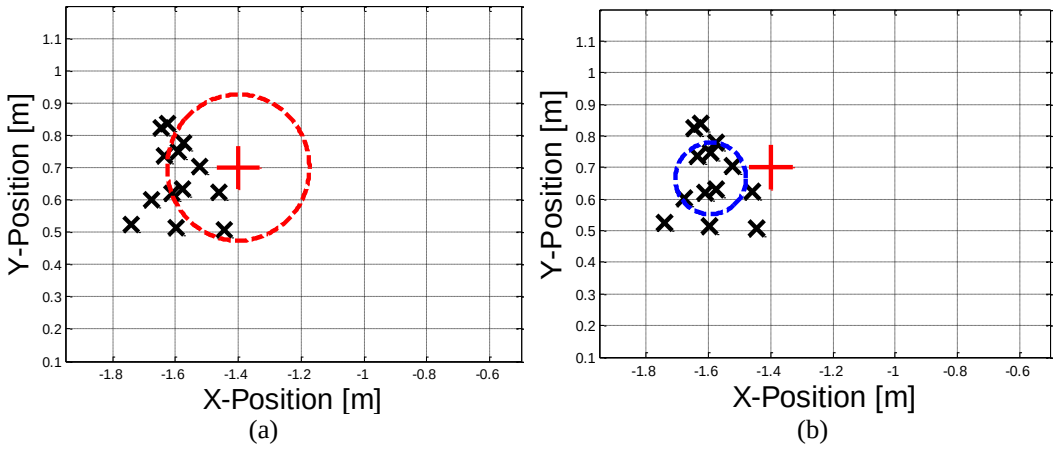

Figure 33. Landing positions of roof top experiment flights in no wind. *(a) Accuracy CEP centered at commanded position (red cross). (b) Precision CEP centered at mean landing position*.

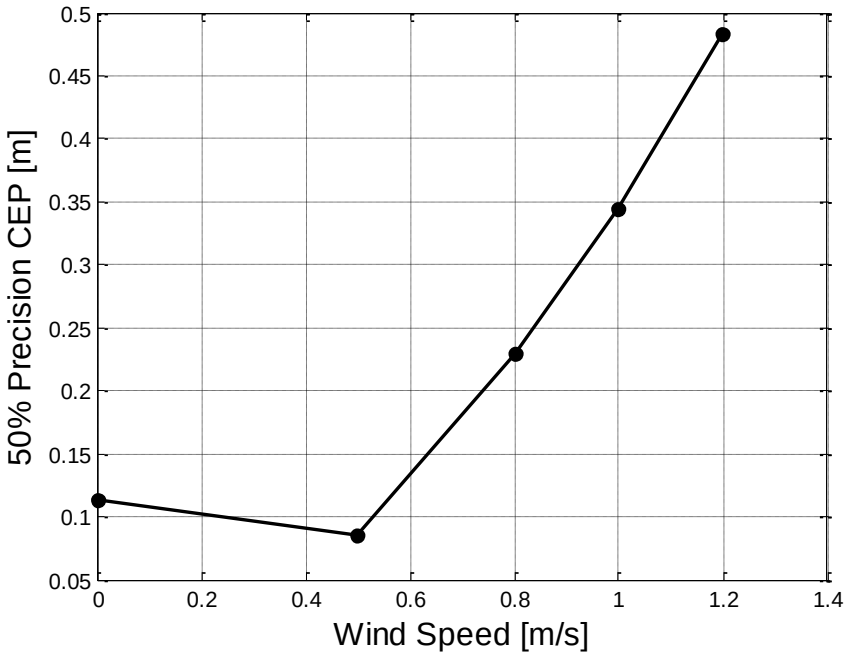

Figure 34. Precision 50% circular error probable of roof top landing experiment.

As seen in Fig. 32, initially the vehicle is blown downwind but after the autopilot compensates for the wind levels the vehicle is able to land close the target position in a steady wind as captured by Figures 32 and 34 and discussed above. These results show the ability of the autopilot to compensate for a steady wind over time. Figure 35 shows example time histories of control inputs at increasing wind levels significantly more control authority required to fly in windy environments.

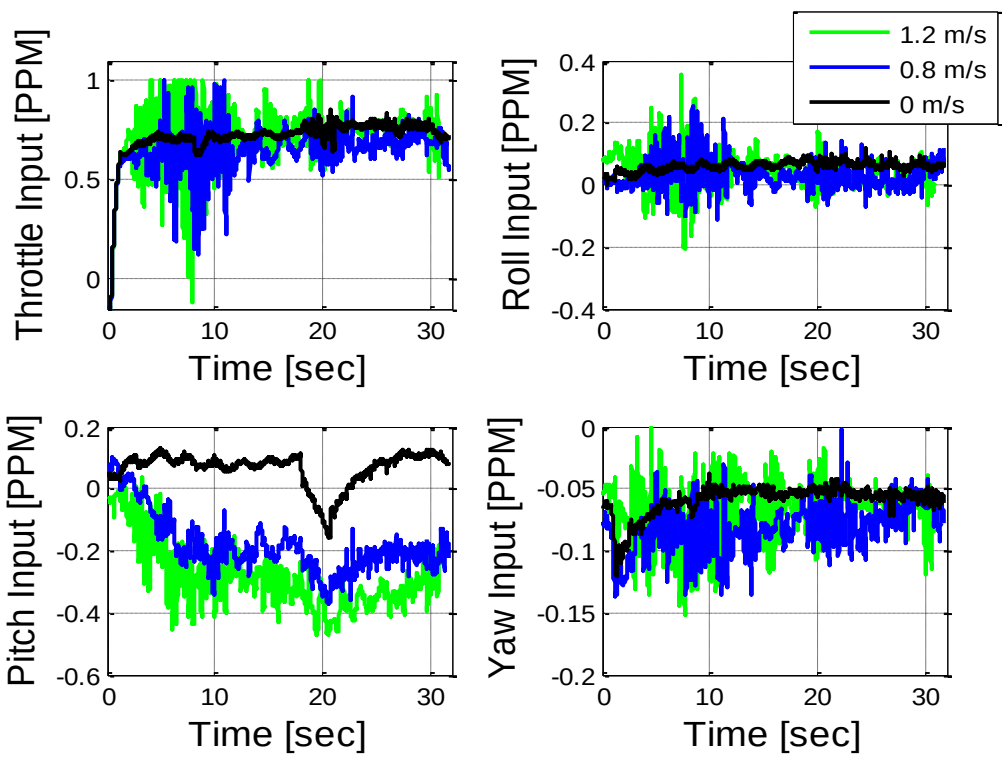

Figure 35. Example time histories of test flight control inputs landing on a roof top in 0.0, 0.8, and 1.2 m/s wind levels.

VI. Future Work

The results of these experiments will be used as benchmarks for continued experimental and computer-simulated studies to identify key vehicle and control law parameters that will improve MAV performance in gusts. Future planned experiments using the micro coaxial helicopter include studies on the effect of controller bandwidth on performance and the changes in power consumption in wind environments. Further experimentation is planned to quantify the performance of different MAV platforms in gusts. Platforms possess inherently different characteristics such as stability and control authority which will lead to different responses in wind environments. Two platforms that will be used for this study are a micro hybrid hopping vehicle and a micro quadrotor.

The Hopping Rotochute (Fig. 36) is a hybrid micro vehicle developed by Georgia Tech. The device consists of a small rotor system housed in a lightweight cage. The vehicle transverses an area by intermittently powering the rotor system allowing the vehicle to hop over obstacles of various shapes and sizes. The Hopping Rotochute's low center of mass causes the vehicle to passively reorient itself to an upright attitude when in contact with ground thus allowing it to robustly explore rough terrain. The limited flight time during hopping may decrease the effects of wind disturbances on the vehicle minimizing tracking error and energy consumption.

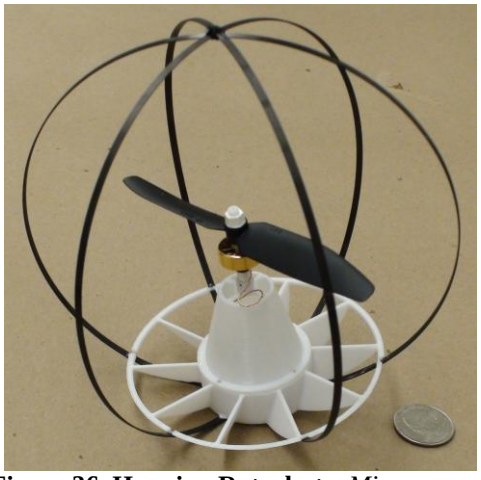

Figure 36. Hopping Rotochute. *Micro hybrid hopping vehicle.*

A micro quad-rotor (Fig. 37) is currently in development to test the performance of a more maneuverable platform with more control authority in gust environments. The platform takes advantage of its inherent instability to enhance controllability and mobility. In contrast to other MAV platforms a quad-rotor can implement all four of its motors as actuators or control inputs. Therefore there is a significant increase in the amount of control authority available in the micro quad-rotor. Thus this micro quad-rotor presents a potential solution for the degradation in performance of MAVs in wind gusts by allowing for quicker responses to deviations from the desired attitude and position. The sensing and actuation requirements necessary to fly an unstable platform on this scale are currently being quantified.

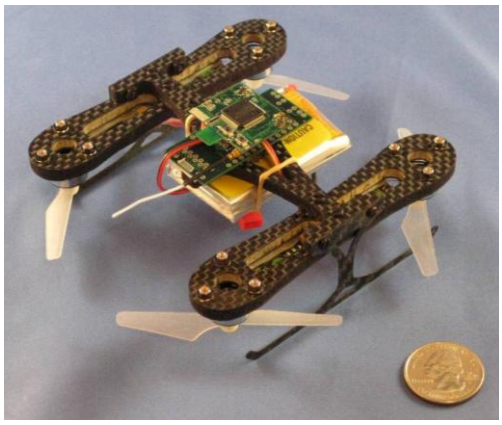

Figure 37. Micro quad-rotor. *In development at the Autonomous Vehicle Laboratory at the University of Maryland.*

VII. Conclusions

A set of experiments was performed to start to understand MAV response to realistic wind environments. In all prototype maneuvers performed—hover, forward flight, and roof top landing—MAV performance degraded in wind conditions and in most cases the decreases were severe. All three experiment types showed some control saturation in throttle which may account from some performance decreases since the autonomous control algorithm does not include any anti-wind up logic; however most decreases in performance were so large that anti-wind up logic will not be the only solution required. The roof top landing experiment showed that the autopilot was able to compensate for a steady wind allowing the helicopter to land close to the target. Also when testing hover capability in turbulent flow the vehicle was observed to be unable to react to quickly changes in wind magnitude (at position 2) leading to crashes due to overcompensation of controls. This shows that increasing controller bandwidth to compensate faster may improve performance in multiple wind environments. Modeling and simulation will be used to identify if these and other changes to vehicle and control law design will improve MAV performance in gusts. The potential applications of MAVs are limited by the environments they can safely operate in thus finding solutions to these issues will be critical moving forward.

References

[1] Costello, M. "Challenges Facing Micro Air Vehicle Flight Dynamics and Controls Engineers," *46th AIAA Aerospace Sciences Meeting and Exhibit*, January 7-10, 2008.

[2] Galinski, C., and Zbikowski, R., "Some Problems of Micro Air Vehicles Development," *Bulletin of the Polish Academy of Sciences: Technical Sciences*, Vol. 55, No. 1, 2007.

[3] Frost, W., and Shahabi, A., "A Field Study of Wind Over a Simulated Block Building," *NASA Technical Report*, NASA CR-2804, March 1977.

[4] http://www.buildingscience.com/documents/digests/bsd-014-air-flow-control-in-buildings?topic=doctypes/digests. viewed on July 7, 2010.

[5] Johnson, E., and Jacob, J., "Development and Testing of a Gust and Shear Tunnel for NAVs and MAVs," *47th AIAA Aerospace Sciences Meeting Including The New Horizons Forum and Aerospace Exposition*, January 5-8, 2009.

[6] Conceicao, E., Vicente, V., and Lucio, M., "Airflow Inside School Building Office Compartments with Moderate Environments," *HVAC&R Research*, Vol 14. No. 2, March 2008.

[7] Etkin, B., "Turbulent Wind and Its Effect on Flight," *Journal of Aircraft*. Vol 19, No. 5, pp 327-345, May 1981.

[8] Lootens, K. J. B., van Paassen, M. M., and Mulder, M., "Flight Path Oriented Control for Large Transport Aircraft. –A Model-Reference Approach," *AIAA Guidance, Navigation, and Control Conference and Exhibit*, August 21-24, 2006.

[9] Hahn, K., and Schwarz, C., "Alleviation of Atmospheric Flow Disturbance Effects on Aircraft Response". *26th International Congress of the Aeronautical Sciences*, 2008.

[10] Etkin, B., *Dynamics of Atmospheric Flight*, Dover Publications, Mineloa, New York, 2000.

[11] Miller, D., de Brun, E., Lu, Y., and Hagar, P., "V-22 Roll-on-Deck Control Law Design," *Journal of the American Helicopter Society*, Vol. 55, No. 2, April 2010.

[12] Mehta, A., and Pister, K., "WARPWING: A complete open source control platform for miniature robots," *2010 IEEE/RSJ International Conference on Intelligent Robots and Systems (IROS 2010)*, October 2010 (to be published).

[13] Ol, M., Parker, G., Abate, G., and Evers, J., "Flight Controls and Performance Challenges for MAVs in Complex Environments," *AIAA Guidance, Navigation, and Control Conference and Exhibit*, August 18-21, 2008.